Chemical Engineering Science 166 (2017) 303–312

Contents lists available at ScienceDirect

Chemical Engineering Science

journal homepage: www.elsevier.com/locate/ces

Numerical study of three-dimensional droplet impact on a flowing liquid film in annular two-phase flow

Zhihua Xie [a,b,c,d,*], Geoffrey F. Hewitt [b], Dimitrios Pavlidis [a], Pablo Salinas [a], Christopher C. Pain [a], Omar K. Matar [b]

[a] Department of Earth Science and Engineering, Imperial College London, UK
[b] Department of Chemical Engineering, Imperial College London, UK
[c] Hydro-environmental Research Centre, School of Engineering, Cardiff University, UK
[d] State Key Laboratory of Coastal and Offshore Engineering, Dalian University of Technology, China

HIGHLIGHTS

- 3D droplet deposition process in annular flow is studied in detail.
- 3D simulation of droplet impacting on flowing liquid film with a shallow angle.
- Atmospheric and high pressure conditions are taken into account for two cases.
- A new CV-FE method is employed for 3D interfacial flows with surface tension.
- The numerical framework also features an anisotropic adaptive mesh algorithm.

ARTICLE INFO

Article history:
Received 10 December 2016
Received in revised form 2 April 2017
Accepted 8 April 2017
Available online 13 April 2017

Keywords:
Adaptive unstructured mesh
Droplet impact
Liquid film
Numerical simulation
Three-dimensional
Two-phase flow

ABSTRACT

Annular flow with liquid entrainment occurs in a wide variety of two-phase flow system. A novel control volume finite element method with adaptive unstructured meshes is employed here to study three-dimensional droplet deposition process in annular two-phase flow. The numerical framework consists of a 'volume of fluid' type method for the interface capturing and a force-balanced continuum surface force model for the surface tension on adaptive unstructured meshes. The numerical framework is validated against experimental measurements of a droplet impact problem and is then used to study the droplet deposition onto a flowing liquid film at atmospheric and high pressure conditions. Detailed complex interfacial structures during droplet impact are captured during the simulation, which agree with the experimental observations, demonstrating the capability of the present method. It is found that the effect of the ambient pressure on the fluid properties and interfacial tension plays an important role in the droplet deposition process and the associated interfacial phenomena.

1. Introduction

Droplet impact on solid or liquid interface is a ubiquitous phenomenon in many engineering applications, such as inkjet printing, spray painting and coating, spray cooling, internal combustion engines, liquid atomization and cleaning (Yarin, 2006). Although this fascinating fluid mechanics problem and its associated phenomena have enjoyed significant attention in the literature, much less attention has been given to droplet impact in annular two-phase flows.

In annular two phase gas-liquid flow, part of the liquid phase flows as a liquid film on the channel walls and the remaining liquid flows as droplets entrained in the gas core of the flow. Droplets are continually being entrained from the film surface and are redeposited back onto the surface. In annular flow, the 'dryout', 'burnout' or Critical Heat Flux (CHF) condition corresponds to the drying out of the liquid film which occurs when the evaporation rate of the film exceeds that required to evaporate liquid flowing along the film from upstream plus the liquid which is transported to the film by deposition of droplets (from those which are entrained in the vapour core of the flow). If the (heated) surface becomes dry, then there is a characteristic upwards excursion of wall temperature which signals the occurrence of the CHF condition. A special case is that of upstream dryout where the CHF condition occurs

* Corresponding author at: Hydro-environmental Research Centre, School of Engineering, Cardiff University, UK.
E-mail address: zxie@cardiff.ac.uk (Z. Xie).

http://dx.doi.org/10.1016/j.ces.2017.04.015
0009-2509/

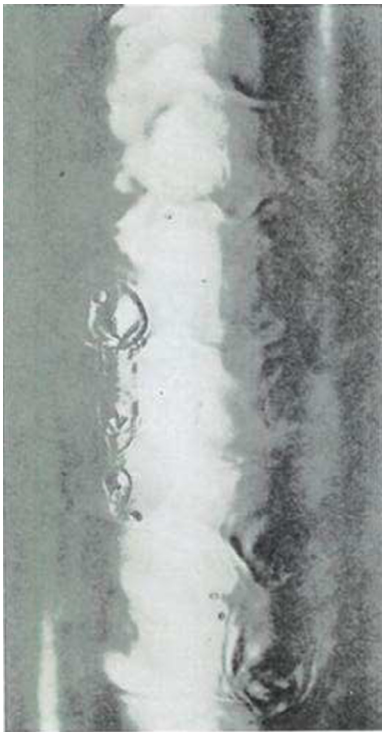

Fig. 1. Experimental picture in annular two-phase flow (Cousins and Hewitt, 1968) of depositing liquid film for a mean gas velocity of 28 m/s.

upstream of the end of the heated section; this situation may occur where the heat flux is decreasing with distance and signifies the existence of a local balance between droplet deposition and evaporation, with the flow of liquid along the film towards the dryout point being zero. One method of measuring the rate of deposition of the droplets is to extract the liquid film and to study the rate of buildup of a new liquid film by subsequent deposition. The new liquid film must, of course, be such that large waves are absent and the entrainment rate is zero. This technique was first employed by Cousins and Hewitt (1968) but was subsequently extended to high mass flow rates by Owen et al. (1985) and by Hewitt and Govan (1990). An alternative method for determination of the rate in heated systems is to determine the position of upstream dryout in a non-uniformly heated tube (Bennett et al., 1967). In the case of the non-uniformly tube and at the upstream location of dryout, there is equality between the rate of evaporation and the rate of deposition. Results obtained by the two methods were in agreement and showed the strong decrease of deposition coefficient with increasing droplet concentration. Hewitt and Govan (1990) correlated both deposition coefficient and entrainment rate and were able to track the change in film flow rate with position in the channel. This allowed prediction of the conditions under which the film flow rate became zero, corresponding to the onset of dryout (at the end of the channel in the case of a uniformly heated channel and, depending on the heat flux distribution, upstream dryout or dryout at the end of the channel). A comprehensive review on the droplets in annular two-phase flow can be found in Azzopardi (1997).

Annular flow with liquid entrainment occurs in a wide variety of two-phase flow system. Only few studies have reported the droplet deposition process for naturally entrained droplets back onto the liquid film. Cousins and Hewitt (1968) reported extensive and detailed measurements of droplet deposition in air-water annular flow and the results suggest that, in the case of deposition in annular flow at low film flow rates, all of the liquid deposited remains attached to the film at the wall. This result is surprising in that droplets are often seen to bounce from a wall liquid layer (as exemplified by droplets impinging on a falling liquid film). The experimental results seem to show that, in the presence of the high gas velocities characteristic of annular flow, the droplets do not bounce: rather, they are more slowly decelerated and leave a streak as they impinge on the film and slow down to be part of the film. The evidence from the experiments (as shown in the example in Fig. 1) is that all the droplets are absorbed into the film. This total absorption is an important feature of models for film dryout. Pham et al. (2014) performed backlit visualisation of gas-sheared liquid film on the outer surface of a cylinder – part of a rod bundle. They presented a number of impact events with formation of a liquid ligament and creation of secondary droplets. Alekseenko et al. (2014) investigated droplet impacts in downward annular flow using laser-induced fluorescence (LIF)-technique in one longitudinal section of the pipe. They have measured maximum depth and width of the craters, created by impacting droplets, together with spreading velocities and typical lifetime in a wide range of experimental conditions. Cherdantsev et al. (2014) studied the three-dimensional wavy structure and liquid entrainment for gas-sheared liquid film in an horizontal rectangular duct. Recently, Cherdantsev et al. (2017) studied droplet impacts in horizontal gas-sheared liquid film using LIF technique. The parameters of impacting droplets and local film thickness were measured in both longitudinal and transverse coordinates with highly-resolved spatial and temporal resolution. Two main scenarios were identified including a crater appears on film surface for large angle impact and a long narrow furrow appears for shallow angle impact.

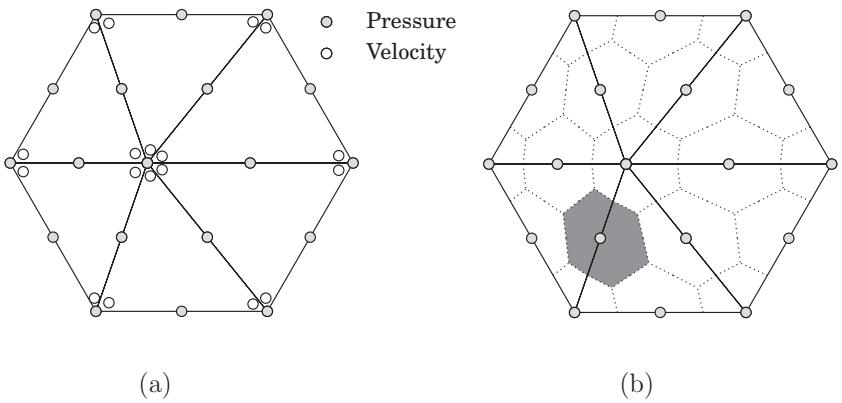

Fig. 2. (a) Finite element used to discretise the fluids equations. The central position of key solution variables are indicated here for the P_1DG-P_2 element pair (Pavlidis et al., 2016); (b) diagram showing the relationship between intersecting control volumes (shaded area) and elements for the P_2 element.

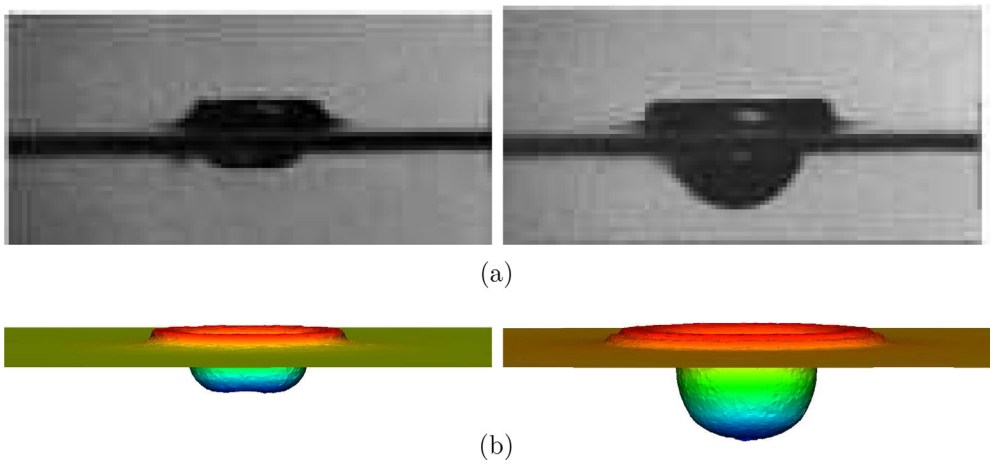

Fig. 3. Comparison of experimental and numerical results for normal impact of a water droplet on a deep water pool. Panel (a) shows the experimental results of Liow (2001) and (b) shows the numerical results for two selected times. This case is characterised by a Froude number $Fr = U/\sqrt{gD} = 14.8$, Weber number $We = \rho U^2 D/\sigma = 134$, where droplet diameter is $D = 2.12$ mm with impacting speed $U = 2.13$ m/s. The gravitational acceleration is $g = 9.8$ m^2/s and the surface tension coefficient $\sigma = 0.072$ N/m. The colour shows the distance normal to the flat air-water interface. (For interpretation of the references to colour in this figure legend, the reader is referred to the web version of this article.)

In terms of modelling and simulations, numerous methods have been proposed and used to simulate two-phase flows (Scardovelli and Zaleski, 1999). Some numerical studies have been undertaken for droplet impact problems, such as droplet impact on a solid surface (Bussmann et al., 2000), normal or oblique (Watanabe et al., 2008) impact on a quiescent deep pool, normal (Yokoi, 2008) or oblique (Ming and Jing, 2015) impact on a static thin film, normal impact on a moving wall with a liquid film (Ming and Jing, 2014). Some detailed interfacial structured have been captured during these studies including splash and crown formation. However, little attention has been given for oblique droplet impact on a *flowing* liquid film.

The objective of the present study is to investigate droplet deposition process described by Cousins and Hewitt (1968) numerically, which acts as a complementary approach for the experimental measurements to provide some detailed information during the impact, including interface coalescence and breakup. As will be seen, the numerical predictions are supportive of the interpretation made by Cousins and Hewitt (1968). The modelling study has also been extended to results for upstream dryout in high pressure steam-water flow and similar results have been obtained. An adaptive unstructured mesh modelling framework is employed here, which is ideal for the capturing and resolution of the multi-scale feature of the flow phenomena associated with the droplet impact problem by reducing computational effort without sacrificing accuracy. To the best of our knowledge, this is the first three-dimensional simulation of an oblique, low-angle, high-speed droplet impact on a flowing liquid film, which corresponds to situations that arise in annular, two-phase flows.

The remainder of this paper is organised as follows. Description of the mathematical model, numerical methods, validation and

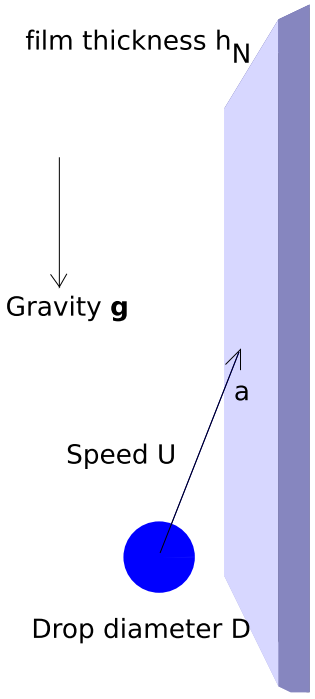

Fig. 4. Schematic of the drop deposition problem.

Table 1
Parameters used to characterise the drop deposition in the two cases studied in the present work.

Variables	Case 1	Case 2
Angle of contact a (°)	5	
Film thickness h_N (m)	6.0×10^{-4}	
Film mean velocity u_N (m/s)	0.6	
Droplet diameter D (m)	3.0×10^{-4}	
Droplet speed U (m/s)	25	
Liquid density (kg/m^3)	1000	740
Liquid viscosity (kg/(m s))	9.892×10^{-4}	9.1×10^{-5}
Ambient fluid density (kg/m^3)	1.125	36.53
Ambient fluid viscosity (kg/(m s))	1.81×10^{-5}	1.9×10^{-5}
Interfacial tension σ (N/m)	0.072	0.018
Froude number $\left(Fr = \frac{U}{\sqrt{gD}}\right)$	461	461
Weber number $\left(We = \frac{\rho U^2 D}{\sigma}\right)$	2604	7805
Eotvos number $\left(Eo = \frac{\Delta\rho g D^2}{\sigma}\right)$	0.012236	0.03490
Morton number $\left(M = \frac{g\mu^4\Delta\rho}{\rho^2\sigma^3}\right)$	2.51×10^{-11}	1.54×10^{-13}
Capillary number $\left(Ca = \frac{\mu U}{\sigma}\right)$	0.3435	0.1280
Ohnesorge number $\left(Oh = \frac{\mu}{\sqrt{\rho\sigma D}}\right)$	6.73×10^{-3}	1.45×10^{-3}

computational setup is given in Section 2. 3D numerical results are presented and discussed in Section 3. Finally, some concluding remarks and future work are given in Section 4.

2. Mathematical model and numerical methods

A multi-fluid modelling framework has been developed based on the multi-component modelling approach with information

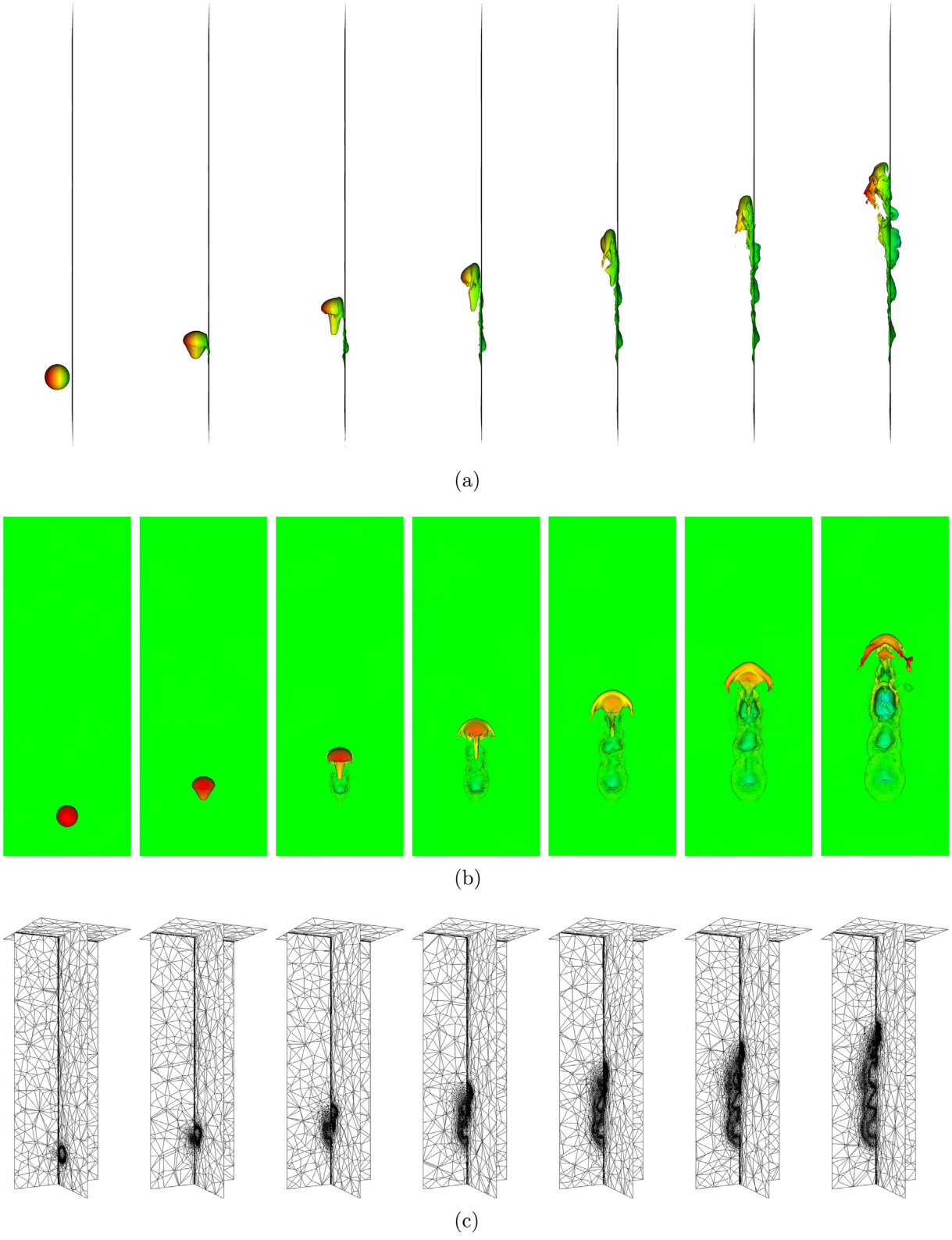

Fig. 5. Snapshots for numerical simulations of the droplet deposition for the air and water case from dimensionless time T^* 0 to 9 with interval of $\Delta T^* = 1.5$. (a) Shows the side view of the simulation whereas (b) shows the front view of the problem, and the associated unstructured meshes on three cut planes are illustrated in (c). The colour shows the distance normal to the thin film. (For interpretation of the references to colour in this figure legend, the reader is referred to the web version of this article.)

on interfaces embedded into the continuity equations. In this section, we first describe the mathematical model and then we present our numerical framework based on the control volume and finite element method. Later a normal droplet impact problem is selected to show the validation and the computational setup is presented last.

2.1. Governing equations

In two-phase flows, let α_i be the mass fraction of phase i, where $i = 1, 2$, the density and dynamic viscosity of phase i are ρ_i and μ_i, respectively. A constraint on the system is:

$$\sum_{i=1}^{2} \alpha_i = 1. \tag{1}$$

For each fluid component i, the conservation of mass may be defined as,

$$\frac{\partial}{\partial t}(\alpha_i) + \nabla \cdot (\alpha_i \mathbf{u}) = 0, \quad i = 1, 2, \tag{2}$$

and the equations of motion of an incompressible fluid may be written as:

$$\frac{\partial(\rho \mathbf{u})}{\partial t} + \nabla \cdot (\rho \mathbf{u} \otimes \mathbf{u}) = -\nabla p + \nabla \cdot [\mu(\nabla \mathbf{u} + \nabla^{\mathrm{T}} \mathbf{u})] + \rho \mathbf{g} + \sigma \kappa \mathbf{n} \delta, \tag{3}$$

where t is the time, $\mathbf{u}$ is velocity vector, p is the pressure, the bulk density is $\rho = \sum_{i=1}^{2} \alpha_i \rho_i$, the bulk dynamic viscosity is $\mu = \sum_{i=1}^{2} \alpha_i \mu_i$, $\mathbf{g}$ is the gravitational acceleration vector, σ is the surface tension coefficient, $\kappa = \nabla \cdot \mathbf{n}$ is the interfacial curvature, $\mathbf{n}$ is the interface unit normal, and δ is the Dirac delta function.

2.2. Numerical methods

The numerical framework consists of a mixed control volume and finite element formulation. In the mixed formulation, the domain is discretised into triangular or tetrahedral elements and in this work, they are $P_1DG\text{-}P_2$ elements (linear discontinuous velocity between elements and quadratic continuous pressure between elements) (Pavlidis et al., 2016). Fig. 2 shows the locations of the degrees of freedom for the $P_1DG\text{-}P_2$ element and the boundaries of the control volumes.

A transient, mixed, control-volume and finite-element formulation is used to discretise the governing equations (Eqs. (2) and (3)). A finite volume discretisation of the continuity equations and a linear discontinuous Galerkin (DG) (Pavlidis et al., 2016) discretisation of the momentum equations are employed with backward Euler time stepping. Within each time-step, the equations are iterated upon using a projection-based pressure determination method until all equations are simultaneously balanced. The main numerical framework includes a finite element type ($P_1DG\text{-}P_2$) for

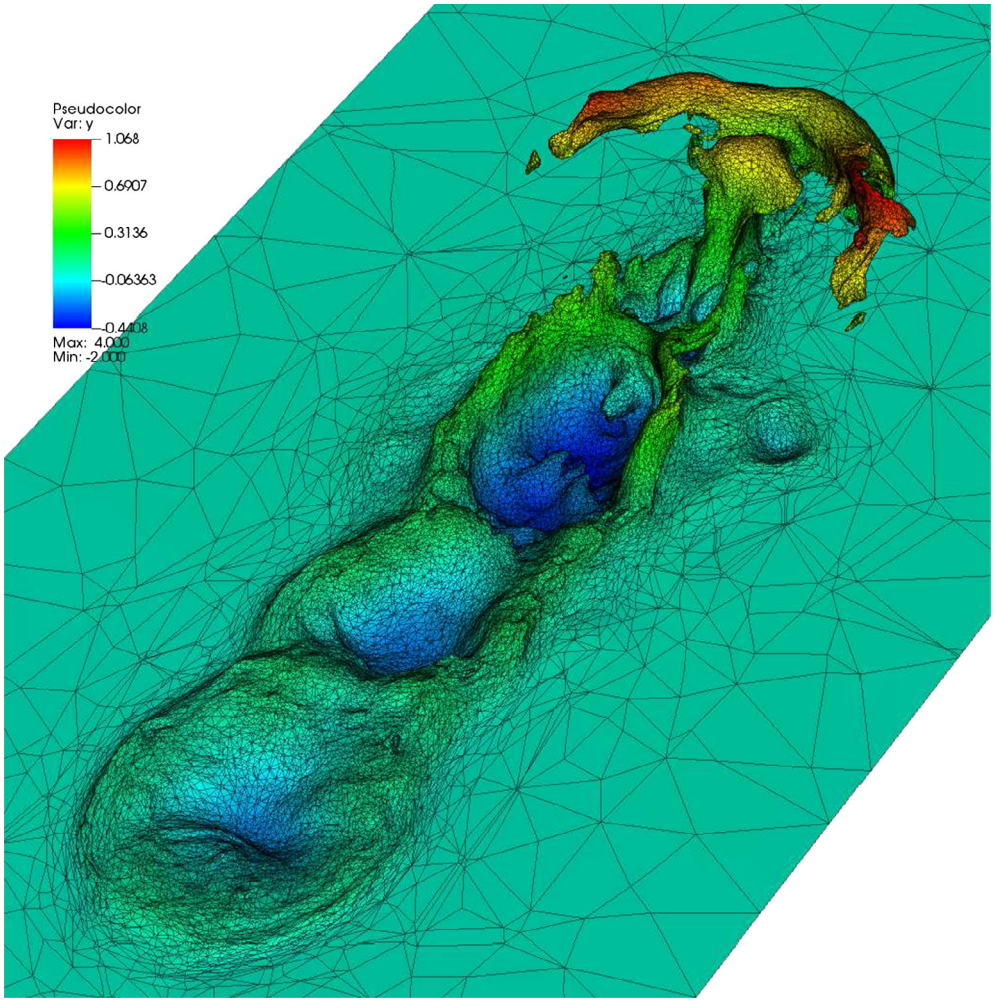

Fig. 6. Zoom in region for the air and water case for the interface structure with colour representing the distance normal to the thin film along with the adaptive unstructured mesh on the interface. (For interpretation of the references to colour in this figure legend, the reader is referred to the web version of this article.)

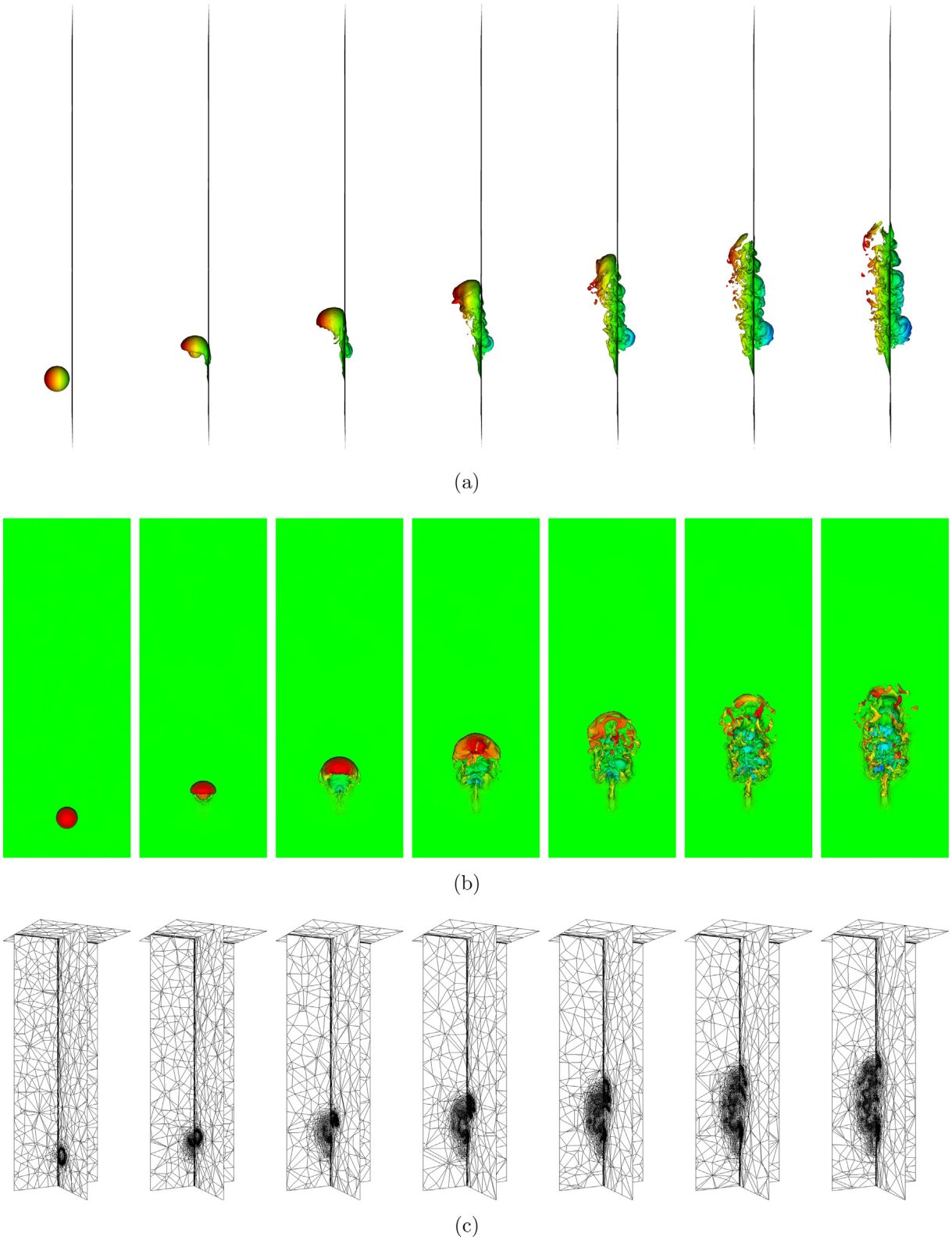

Fig. 7. Snapshots for numerical simulations of the droplet deposition for the steam and water case at a high pressure (70 bar) condition from dimensionless time T^* 0 to 9 with interval of $\Delta T^* = 1.5$. (a) Shows the side view of the simulation whereas (b) shows the front view of the problem, and the associated unstructured meshes on three cut planes are illustrated in (c). The colour shows the distance normal to the thin film. (For interpretation of the references to colour in this figure legend, the reader is referred to the web version of this article.)

multi-fluid flow problems, which ensures exact balance between buoyancy force and pressure gradient. The framework also features a novel interface capturing scheme based on compressive control volume advection method (Pavlidis et al., 2016), involving a high-order accurate finite element method to obtain fluxes on the control volume boundaries, where these fluxes are subject to

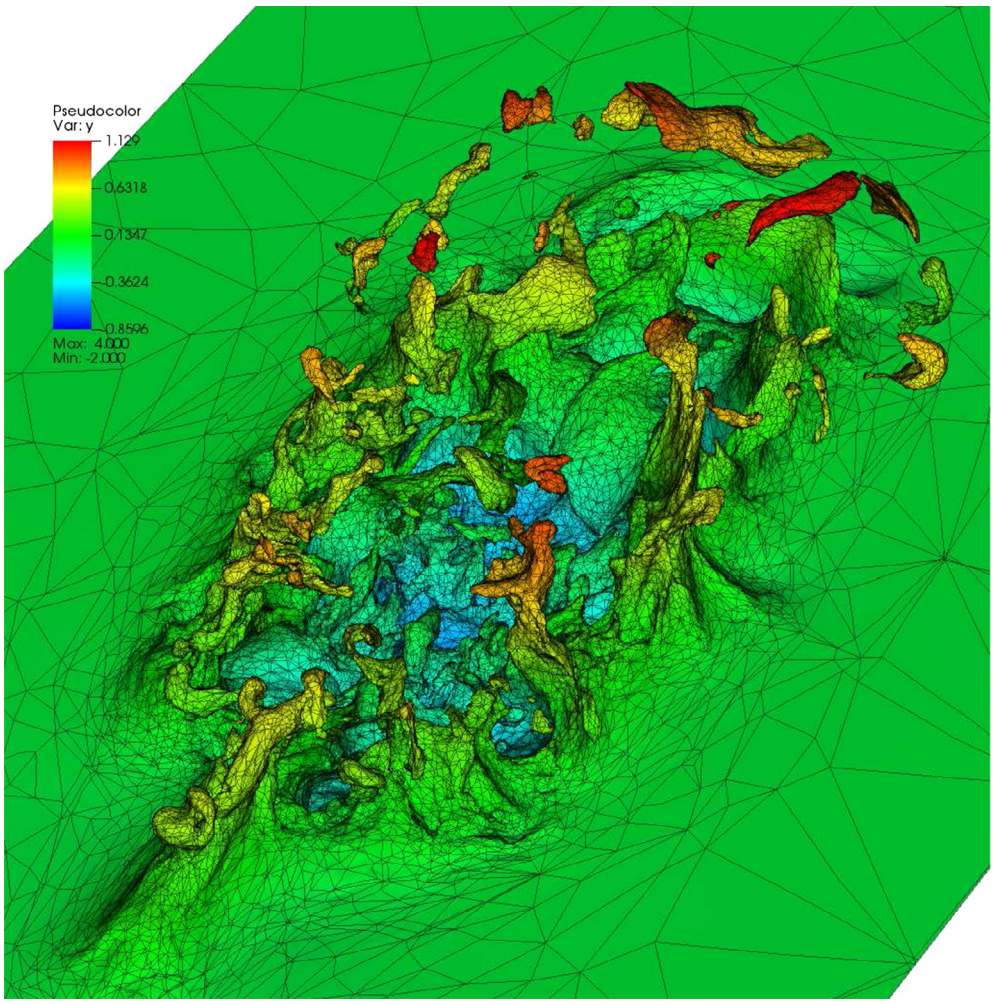

Fig. 8. Zoom in region for the steam and water case for the interface structure with colour representing the distance normal to the thin film along with the adaptive unstructured mesh on the interface. (For interpretation of the references to colour in this figure legend, the reader is referred to the web version of this article.)

flux-limiting using a normalised variable diagram approach (Leonard, 1991) to obtain bounded and compressive solutions for the interface. The implementation of capillary/surface tension force in the framework using an unstructured mesh minimises spurious velocities often found in interfacial flows (Xie et al., 2016). Finally, use of anisotropic unstructured mesh adaptivity (Pain et al., 2001) allows the grid resolution to be concentrated in relatively important regions, such as the vicinity of interfaces, while lower resolution can be used in other regions; this leads to a significant gain in computational efficiency without sacrificing accuracy.

2.3. Validation

The numerical framework has been employed to study various multiphase flow problems for inertia-dominated (Xie et al., 2014, 2016; Pavlidis et al., 2014, 2016; Percival et al., 2014) as well as porous media (Gomes et al., 2017; Salinas et al., in press-b, in press-a) flows. The detailed modelling of three-dimensional bubbles, droplet and liquid films can be found in Xie et al. (2016). Here we simulate a case for normal impact of a water droplet on a deep water pool to demonstrate the capability of the present framework in modelling droplet impact problems. Fig. 3 shows a comparison between the experimental measurements (Liow, 2001) and present simulations with the same parameters, where a water droplet with the diameter of $D = 2.12$ mm impacts a water pool whose depth far exceeds D with a speed of $U = 2.13$ m/s. The Froude number, $Fr = U/\sqrt{gD}$, and Weber number, $We = \rho U^2 D/\sigma$, for this case are 14.8 and 134, respectively. It can be seen from Fig. 3 that a good qualitative agreement is obtained between the experimental and numerical results. The simulation has also been quantitatively compared with the experiment and it is found that the predicted cavity depth is $1.4D$, which is very close to the experimental measurement of $1.5D$ after 4 ms of the initial impact in the right panel of Fig. 3; this inspires confidence in the accuracy and reliability of the numerical methods used to cary out the computations. Additional validation of the numerics will be provided via further comparisons with experimental data in Section 3.

2.4. Computational setup

Droplet deposition is a complex phenomenon and may depend on the way in which the droplets are entrained and on the film flow conditions, and in particular the gas velocity, the wave structure, the upstream conditions and impingement angle. In order to investigate the deposition process, a droplet impact on a flat moving film is considered in the present study and the schematic is shown in Fig. 4. Initially, a droplet with a diameter of D moves with a constant speed U towards the flowing film with an angle of a to the vertical. The thickness of the film is h_N and the film is moving upwards with a mean velocity u_N. For this simulation, we use a

relatively large computational domain $16D \times 6D \times 6D$ to avoid boundary effects. The adaptive criteria is based on the curvature of the interface and the minimum length $h_{min} = 0.03D$ is set in the computation. Based on the experimental measurement in Cousins and Hewitt (1968), two cases with different fluid properties, reflecting atmospheric and high pressure (70 bar) situations, are studied with the parameters given in Table 1.

3. Results and discussion

In the present study, results are presented in dimensionless form using the droplets initial diameter D to normalise positions and thickness, while velocities and times are normalised by the droplet initial speed U and temporal scale D/U, respectively.

We first consider the droplet impact in an air and water system at atmospheric pressure conditions. Snapshots of the numerical results for the droplet deposition are shown in Fig. 5. Side- and top-views are presented in Fig. 5(a) and (b) in order to illustrate the shape of the interface. The fully-adaptive, unstructured meshes that during the evolve droplet impact dynamics are also shown in Fig. 5(c). It can be seen that there is a deformation of the shape of the droplet when it approaches the base film. The deformation is larger on the back of the droplet with a cone shape. When the bottom of the droplet touches the base film, a dimple is generated and spreads in the spanwise direction. The front of the droplet deforms into a horseshoe shape while its tail impacts on the base film to generate several dimples. It can be also seen that the mesh is adaptive during the simulation; the mesh is refined in the vicinity of the air–water interface to resolve the detailed structure, and coarsened elsewhere for computational efficiency. The mesh-refined region is gradually increased due to the complex structures generated during the droplet impact. It can be seen that the numerical predictions are supportive of the interpretation made by Cousins and Hewitt (1968) that in the presence of the high gas velocities characteristic of annular flow, the droplets do not bounce: rather, they are more slowly decelerated and leave a streak as they impinge on the film and slow down to be part of the film.

Fig. 6 shows the zoom in region of the interface structure for the air and water case and the fully unstructured mesh on the interface. It can be seen that finer mesh is placed in the region where there is large topology change. The wavy surface and entrainment of small droplets are captured in the simulation.

Next we consider the droplet impact in a steam and water system at a high pressure (70 bar) situation. As it can be seen from Table 1, at higher pressure situation, both the density and viscosity of the water decrease, whereas the density and viscosity increase for the ambient fluid (steam). And also the interfacial tension coefficient decreases at higher pressure. The simulation is initialised exactly the same as the first case and only fluid properties are changed corresponding to the steam and water system. Some snapshots for the numerical results for the droplet deposition at high pressure are shown in Fig. 7. It can be seen that the predicted results are significantly different from the previous case. A canopy shape is developed at the front of the droplet and there is no formation of long tail at the back of the droplet when compared to the previous case. When the bottom of the droplet touches the base film, a large dimple is generated. The thickness of the canopy decreases during the evolution and eventually the canopy breaks up into several ligaments and droplets. In this case, the water droplet travels less far away compared to the previous case due to less

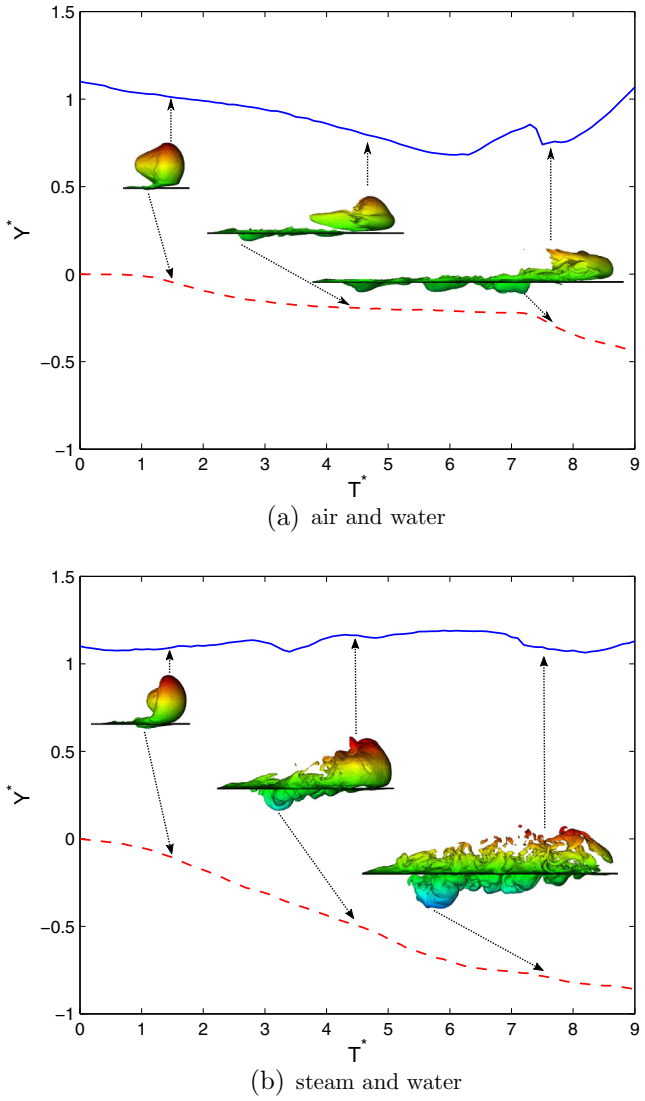

Fig. 9. History of highest (blue solid line) and lowest (red dash line) point location normal to the film during the simulation for (a) air and water system and (b) steam and water system. The time and film thickness have been normalised by D/U and D. (For interpretation of the references to colour in this figure legend, the reader is referred to the web version of this article.)

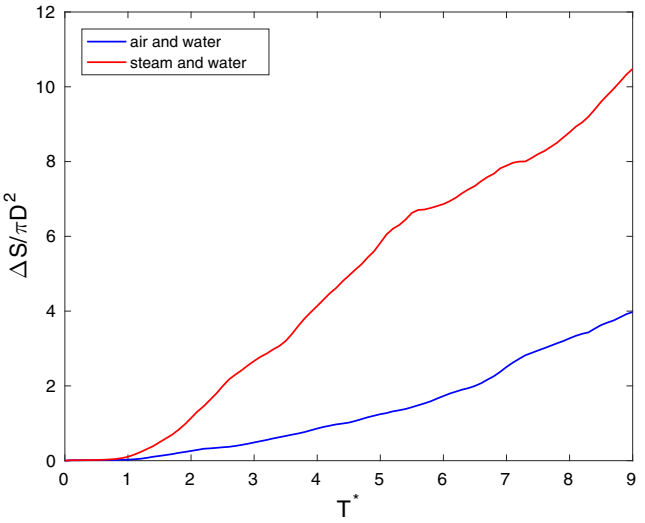

Fig. 10. Temporal variation of the normalised change in the interfacial area from its initial value associated with the air-water, and steam-water cases. The time and the increase surface area compared to the initial condition ($\Delta S = S - S_{t=0}$) have been normalised by D/U and the droplet surface area πD^2.

momentum associated with the water droplet at the high pressure condition.

Fig. 8 shows the zoom in region of the interface structure for the steam and water case and the fully unstructured mesh on the interface. It can be seen that both the base film and the top droplet have very complex interfacial structures. Due to the decrease of the interfacial tension, the droplet breaks earlier to create some ligaments and smaller droplets. All the detailed interfacial structures have been captured in the present simulation, which demonstrates the capability of the present code in dealing with multi-scale multiphase flow problems.

In order to track the interface location during impact, the time history of the highest and lowest interface location normal to the base film is shown in Fig. 9. It can be seen that the two cases are slightly different. For the air and water case, the top interface gradually decreases as the main part of the droplet sinks to the base film. At approximate $T^* = 6$, the horseshoe shape interface is formed at the front of the droplet and the highest points starts to increase. The bottom interface moves downwards when the droplet hit the base film and several steps can be observed from the lowest point profile which is corresponding to the dimples generated during the impact. However for the steam and water case, the level to top interface does not change too much as the droplet breaks up to generate several smaller droplet at the same level. There is no sharp change for the lowest point profile as only one large dimple region is generated during the impact. It can be seen that the droplet penetrates much deeper at a high pressure condition.

It is worth mentioning that the interfacial shape for the two cases studied (air and water: $We = 2604$, $Eo = 0.012236$, $M = 2.51 \times 10^{-11}$, $Ca = 0.3435$, $Oh = 6.73 \times 10^{-3}$; steam and water: $We = 7805$, $Eo = 0.03490$, $M = 1.54 \times 10^{-13}$, $Ca = 0.1280$, $Oh = 1.45 \times 10^{-3}$) is different. In order to illustrate this, we plot in Fig. 10 the interfacial area associated with each case normalised by the single, undeformed droplet surface area, πD^2. It can be seen that before the droplet impact (around $T^* = 1$), there is no change for the interface surface area, which is expected. After impact, the interfacial area for both cases gradually increases due to the generation of complex interfacial structures. However, the increase of the interfacial area for the steam and water case is much higher, with its value of 10.5 compared to the value of 4 for the air and water case. It is noted that this difference of the interface surface area could lead to different heat transfer in annular two-phase flows.

4. Conclusions

In this paper, a control volume finite element method with adaptive anisotropic unstructured meshes has been used for three-dimensional two-phase flows with surface tension, which can modify and adapt unstructured meshes to better represent the underlying physics of interfacial problems and reduce computational effort without sacrificing accuracy.

The numerical framework has been employed to study the droplet deposition problem, in which a single droplet is impacting onto the flowing liquid film, often occurring in annular flows. Complex interfacial structures during droplet impact have been captured by the present method and the numerical predictions are supportive of the interpretation made by Cousins and Hewitt (1968). In addition, two cases with different ambient pressure conditions have been considered in this study and it is shown that the fluid properties and interfacial tension can have significant effects on the deposition process and the shape of the interfacial structures.

As droplet impact problem is very complex only a single droplet impact event has been study here. Future work will focus on the study of gas-sheared liquid film, which includes entrainment of droplets from the liquid film and its deposition process back onto the film surface.

Acknowledgements

We would like to thank the EPSRC MEMPHIS multiphase Programme Grant (number EP/K003976/1) for helping to fund this work. Dr. D. Pavlidis would like to acknowledge the support from the EPSRC UK-Japan Civil Nuclear Energy project Reactor Core-Structure Relocation Modelling for Severe Nuclear Accident (EP/M012794/1) and H2020 In-Vessel Melt Retention. Funding for Dr. P. Salinas from ExxonMobil is gratefully acknowledged. Dr. Z. Xie would also like to acknowledge the financial support by the Open Awards of the State Key Laboratory of Coastal and Offshore Engineering at Dalian University of Technology in China.

References

Alekseenko, S.V., Cherdantsev, A.V., Markovich, D.M., Rabusov, A.V., 2014. Investigation of droplets entrainment and deposition in annular flow using LIF technique. Atomization and Sprays 24 (3), 193–222.
Azzopardi, B., 1997. Detailed observations of wavy interface behaviors of annular two-phase flow on rod bundle geometry. Int. J. Multiph. Flow 23, 1–53.
Bennett, A.W., Hewitt, G.F., Kearsey, H.A., Keeys, R.K.F., Pulling, D.J., 1967. Studies of burnout in boiling heat transfer. Trans. Inst. Chem. Eng. 45, 319–333.
Bussmann, M., Chandra, S., Mostaghimi, J., 2000. Modeling the splash of a droplet impacting a solid surface. Phys. Fluids 12, 3121.
Cherdantsev, A.V., Hann, D.B., Azzopardi, B.J., 2014. Study of gas-sheared liquid film in horizontal rectangular duct using high-speed LIF technique: three-dimensional wavy structure and its relation to liquid entrainment. Int. J. Multiph. Flow 67, 52–64.
Cherdantsev, A.V., Hann, D.B., Hewakandamby, B.N., Azzopardi, B.J., 2017. Study of the impacts of droplets deposited from the gas core onto a gas-sheared liquid film. Int. J. Multiph. Flow 88, 69–86.
Cousins, L.B., Hewitt, G.F., 1968. Liquid Phase Mass Transfer in Annular Two-phase Flow: Droplet Deposition and Liquid Entrainment Technical Report AERE-5657. Chemical Engineering and Process Technology Division, Atomic Energy Research Establishment, Harwell, UK.
Gomes, J.L.M.A., Pavlidis, D., Salinas, P., Xie, Z., Percival, J.R., Melnikova, Y., Pain, C.C., Jackson, M.D., 2017. A force-balanced control volume finite element method for multi-phase porous media flow modelling. Int. J. Numer. Methods Fluids 83, 431–445.
Hewitt, G.F., Govan, A.H., 1990. Phenomena and prediction in annular two-phase flow. In: Kim, J.H., Rohatgi, U.S., Hashemi, A. (Eds.), Symposium on Advances in Gas-Liquid Flows. The American Society of Mechanical Engineers, pp. 41–56.
Leonard, B.P., 1991. The ULTIMATE conservative difference scheme applied to unsteady one-dimensional advection. Comput. Methods Appl. Mech. Eng. 88, 17–74.
Liow, J.L., 2001. Splash formation by spherical drops. J. Fluid Mech. 427, 73–105.
Ming, C., Jing, L., 2014. Lattice boltzmann simulation of a drop impact on a moving wall with a liquid film. Comput. Math. Appl. 67, 307–317.
Ming, C., Jing, L., 2015. A numerical study on splash of oblique drop impact on wet walls. Comput. Fluids 115, 11–24.
Owen, D.G., Hewitt, G.F., Bott, T.R., 1985. Equilibrium annular flows at high mass fluxes: data and interpretation. Physicochem. Hydrodyn. 6, 115–132.
Pain, C.C., Umpleby, A.P., de Oliveira, C.R.E., Goddard, A.J.H., 2001. Tetrahedral mesh optimisation and adaptivity for steady-state and transient finite element calculations. Comput. Methods Appl. Mech. Eng. 190, 3771–3796.
Pavlidis, D., Gomes, J.L.M.A., Xie, Z., Percival, J.R., Pain, C.C., Matar, O.K., 2016. Compressive advection and multi-component methods for interface-capturing. Int. J. Numer. Methods Fluids 80, 256–282.
Pavlidis, D., Xie, Z., Percival, J.R., Gomes, J.L.M.A., Pain, C.C., Matar, O.K., 2014. Two- and three-phase horizontal slug flow modelling using an interface-capturing compositional approach. Int. J. Multiph. Flow 67, 85–91.
Percival, J.R., Pavlidis, D., Xie, Z., Gomes, J.L.M.A., Sakai, M., Shigeto, Y., Takahashi, H., Matar, O.K., Pain, C.C., 2014. Control volume finite element modelling of segregation of sand and granular flows in fluidized beds. Int. J. Multiph. Flow 67, 191–199.
Pham, S.H., Kawara, Z., Yokomine, T., Kunugi, T., 2014. Detailed observations of wavy interface behaviors of annular two-phase flow on rod bundle geometry. Int. J. Multiph. Flow 59, 135–144.
Salinas, P., Pavlidis, D., Xie, Z., Adam, A., Pain, C.C., Jackson, M.D., in press-a. Improving the robustness of the control volume finite element method with application to multiphase porous media flow. Int. J. Numer. Methods Fluids. http://dx.doi.org/10.1002/fld.4381.
Salinas, P., Pavlidis, D., Xie, Z., Pain, C.C., Jacquemyn, C., Melnikova, Y., Jackson, M.D., in press-b. Improving the convergence behaviour of a fixed-point-iteration

solver for multiphase flow in porous media. Int. J. Numer. Methods Fluids. http://dx.doi.org/10.1002/fld.4357.
Scardovelli, R., Zaleski, S., 1999. Direct numerical simulation of free-surface and interfacial flow. Annu. Rev. Fluid Mech. 31, 567–603.
Watanabe, Y., Saruwatari, A., Ingram, D.M., 2008. Free-surface flows under impacting droplets. J. Comput. Phys. 227, 2344–2365.
Xie, Z., Pavlidis, D., Percival, J.R., Gomes, J.L.M.A., Pain, C.C., Matar, O.K., 2014. Adaptive unstructured mesh modeling of multiphase flows. Int. J. Multiph. Flow 67, 104–110.
Xie, Z., Pavlidis, D., Salinas, P., Percival, J.R., Pain, C.C., Matar, O.K., 2016. A balanced-force control volume finite element method for interfacial flows with surface tension using adaptive anisotropic unstructured meshes. Comput. Fluids 138, 38–50.
Yarin, A.L., 2006. Drop impact dynamics: splashing, spreading, receding, bouncing. Annu. Rev. Fluid Mech. 38, 159–192.
Yokoi, K., 2008. A numerical method for free-surface flows and its application to droplet impact on a thin liquid layer. J. Sci. Comput. 35, 372–396.